FLOMEKO2019
18th International Flow Measurement Conference
Portugal | Lisbon | LNEC | 26-28 june 2019

Calculation of the flow-rate measurement uncertainty by means of Pitot tubes using the Monte Carlo Method

L. L. Martins[1], A. S. Ribeiro[1], J. Alves e Sousa[2]

[1]LNEC – National Laboratory for Civil Engineering, Avenida do Brasil, 101, 1700-066, Lisbon, Portugal
[2]IPQ – Portuguese Institute for Quality, Rua António Gião 2, 2829-513 Caparica, Portugal
E-mail (corresponding author): lfmartins@lnec.pt

Abstract

This paper is dedicated to the flow-rate measurement uncertainty calculation, considering the use of Pitot tubes inside closed conduits as the applied measurement method, according to the guidelines and procedures established by the current ISO 3966 standard. The performed study aims the comparison between measurement uncertainties obtained by the conventional error approach mentioned in the method's standard and the results obtained from the application of the Monte Carlo Method (MCM). Using the same input data, a difference of 0,3% was obtained between the 95% relative expanded measurement uncertainties. The obtained probability density function of the compressibility correction factor showed a non-Gaussian asymmetric shape, however, not affecting the remaining quantities in the uncertainty propagation chain. The Pitot tube's calibration factor and the turbulence and high frequency fluctuations were identified as the main uncertainty contributions for the combined measurement uncertainties.

1. Introduction

Pitot tubes are frequently used in several scientific, technical and industrial areas, aiming the measurement of fluid flow, for example, in closed conduits. The normative framework of this measurement method is currently established in ISO 3966 [1], which addresses all the main topics related to the design and maintenance of Pitot static tubes, and describes the calculation procedures of local velocities from measured differential pressures and of the flow-rate by velocity integration.

In particular, this international standard describes a conventional approach based on the error evaluation method, in order to assess the accuracy of the volume flow-rate measurement, providing a detailed formulation of error sources related to the local velocity measurement and flow-rate calculation, being given an example of estimation of the overall uncertainty in its Annex G.

The main motivation of this study is to review and update the procedure used to evaluate the measurement accuracy in flow-rate measurements using Pitot tubes, considering the international documents published after ISO 3966:2008, namely, the latest edition of VIM [2] and GUM Supplements [3-5], widely accepted for complex and nonlinear models such as those required to the studies in this field of knowledge.

The paper is focused on the application of the Monte Carlo Method (MCM) as the proper approach to estimate the measurement uncertainty, due to the non-linearity and complexity of the mathematical models needed to describe the measurand and procedures involved in the velocity computation, integration and corrections.

The performed numerical simulations by MCM are based on a robust pseudo-random number generator and validated computational routines are used for determining the measurement uncertainties and its computational accuracy levels, following the main guidelines of the GUM Supplement 1 [4]. As result, the estimates are obtained within related measurement uncertainties and probability distribution functions, allowing to find the main individual contributions for the output dispersion of local velocity and flow-rate. The use of the input information shown in Annex G of [1] in the simulations, will allow a robust comparison with the results obtained using the conventional error approach.

Section 2 summarizes the mathematical models applied in calculation of the local and discharge velocities and flow-rate quantities. In Section 3, the measurement uncertainty evaluation is described, namely, the probabilistic formulation of input quantities, the uncertainty propagation stages and details about the MCM numerical simulation. The obtained results are shown in Section 4, while in Section 5, conclusions are drawn about the suitability of the MCM approach for the calculation of velocity and flow-rate measurement uncertainty and giving a contribution to be considered in future revision of ISO 3966:2008 [1], namely, of its metrological contents.

2. Velocity and flow-rate measurements by means of Pitot tubes

2.1 Introduction

Pitot tubes are key elements in the measurement of flow (more extensively used gases, rather than in liquids) in closed conduits, being one of the so-called point velocity methods such as those supported by hot-wire and hot-film anemometers, vane anemometers, current meters and laser velocimetry [6]. In this method, several local velocity determinations (sub-section 2.2) are taken across a known cross-section, A, of the fluid stream, which are then spatially integrated in order to known the discharge velocity, U, (sub-section 2.3). The product of these two quantities allows the indirect measurement of the volumetric flow-rate q_V. The additional multiplication by the fluid density, ρ , allows knowing the mass flow-rate, q_m .

2.2 Local velocity

The application of the Bernoulli's principle to the case of a Pitot static tube, allows to express the local fluid velocity, v, at a certain point inside a closed conduit, by

$$v = \alpha \cdot \sqrt{\frac{2 \cdot \Delta p}{\rho}}, \tag{1}$$

where α is the calibration factor of the Pitot tube and Δp is the differential pressure between the total and static pressures. The estimate of the calibration factor is equal to one for standard measurement conditions and Pitot tubes [6], and velocities above 5 m·s^{-1}. Differential pressure is usually measured using a micromanometer connected to the Pitot tube. This measurement is slightly overestimated and can be corrected for head loss, ξ, due to the distance between the static (located downstream) and the total pressure tappings. Its estimate is generally negligible, being equal to the friction head loss in the conduit over the above mentioned distance [1].

The density of a compressible fluid is determined by

$$\rho = \frac{p \cdot M}{Z \cdot R_g \cdot T}, \tag{2}$$

where p is the local static pressure, R_g, is the molar constant of gas, M is the molar mass of the fluid, Z is the gas law deviation factor and T is the local static temperature.

In the case of compressible fluids such as air, namely for velocities above 60 m·s^{-1} [6], expression (1) must include an additional compressibility correction factor, $(1-\varepsilon)$, originating the following expression

$$v = \alpha \cdot (1-\varepsilon) \cdot \sqrt{\frac{2 \cdot \Delta p}{\rho}}. \tag{3}$$

According to [1] and considering low Mach numbers, the compressibility correction factor, $(1-\varepsilon)$, is almost equal to

$$(1-\varepsilon) \approx \left[1 - \frac{1}{2 \cdot \gamma} \cdot \frac{\Delta p}{p} + \frac{\gamma - 1}{6 \cdot \gamma^2} \left(\frac{\Delta p}{p}\right)^2\right]^{\frac{1}{2}}, \tag{4}$$

where γ is the ratio of specific heat capacities, usually varying between 1,1 and 1,7.

2.3 Discharge velocity

The discharge velocity, U, is mathematically defined by the spatial integration of the fluid velocity in the conduit's circular or rectangular measuring cross-section. For this purpose, several standard methods are available [1], being briefly described in Table 1.

Table 1: Methods for the discharge velocity determination.

Graphical integration	A graphical representation of the velocity profile is performed in order to determine the area under the curve which is bounded by the measuring points closest to the conduit wall. The velocity profile in the peripheral zone is assumed to satisfy a power law and is taken into account. No specific location for the measuring points is defined.
Numerical integration	Similar to the previous method with the exception of the velocity profile which is defined by an algebraic curve and integration is performed analytically.
Arithmetical methods	The velocity distribution assumes a particular law and the discharge velocity is given by a linear combination of individual velocities measured at specific locations.

3. Measurement uncertainty evaluation

3.1 Input probabilistic formulation and uncertainty propagation stages

In the flow-rate measurement uncertainty evaluation, four propagation stages are defined: (i) the fluid density; (ii) the local fluid velocity; (iii) the volumetric flow-rate; (iv) the mass flow-rate.

Table 2 presents the probabilistic formulation of the uncertainty components related to the input quantities, based on the standard information [1, 9] and experimental knowledge about the performed measurements.

Table 2: Uncertainty components related to input quantities.

Uncertainty component	Uncertainty source	PDF*	Standard uncertainty
$u(p)$	Local static pressure	Gaussian	100 Pa
$u(M)$	Molar mass of the fluid	Gaussian	$2{,}3\cdot10^{-6}$ kg·mol^{-1}
$u(Z)$	Gas deviation factor	Uniform	0,000 5/√3
$u(R_g)$	Molar constant of gas	Gaussian	$4{,}8\cdot10^{-6}$ J·mol^{-1}·K^{-1}
$u(T)$	Local static temperature	Gaussian	0,1 K
$u(\Delta p)_{\text{inst}}$	Instrumental uncertainty	Gaussian	0,4%
$u(\Delta p)_{\text{head}}$	Correction for head loss	Gaussian	0,2%
$u(\alpha)$	Calibration factor of the Pitot tube	Gaussian	0,2%
$u(\gamma)$	Ratio of specific heat capacities	Uniform	0,3/√3
$u(A)$	Cross-section area	Gaussian	0,2%

*PDF – Probability Density Function.

In the case of the local velocity and volumetric flow-rate quantities, in addition to the measurement uncertainty propagated through the corresponding mathematical models, additional uncertainty components are introduced (see Table 3 for the local velocity and Table 4 for the volumetric flow-rate), based on the information shown in Annex G of [1].

Table 3: Additional uncertainty components related to the local velocity measurement.

Uncertainty component	Uncertainty source	PDF	Standard uncertainty
$u(v)_{\text{block}}$	Blockage effect	Gaussian	0,25%
$u(v)_{\text{high}}$	Turbulence and high frequency fluctuations	Gaussian	0,50%
$u(v)_{\text{incl}}$	Pitot tube inclination	Gaussian	0,15%
$u(v)_{\text{grad}}$	Gradient velocity	Gaussian	0,15%
$u(v)_{\text{slow}}$	Slow fluctuations	Gaussian	0,10%

Table 4: Additional uncertainty components related to the volumetric flow-rate measurement.

Uncertainty component	Uncertainty source	PDF	Standard uncertainty
$u(q_V)_{\text{integ}}$	Integration technique	Gaussian	0,10%
$u(q_V)_{\text{rough}}$	Roughness coefficient estimate	Gaussian	0,05%
$u(q_V)_{\text{point}}$	Insufficient number of points	Gaussian	0,10%
$u(q_V)_{\text{posit}}$	Pitot tube positioning	Gaussian	0,05%

The results shown in Section 4 are based on typical estimates values (Table 5) of the mentioned input quantities in the flow-rate measurement by means of Pitot tubes, considering air as the fluid inside the closed conduit.

Table 5: Estimates related to the input quantities.

p	105 000 Pa	γ	1,40
M	28 963,5 ·10^{-6} kg·mol^{-1}	Δp	10,00 Pa
Z	1,000 00	ξ	0,00 Pa
R_g	8,314 459 8 J·mol^{-1}·K^{-1}	α	1,000
T	290,0 K	A	0,120 0 m^2

3.2 Monte Carlo Method

The computational simulation algorithm was developed in Matlab®, following the guidelines of Supplement 1 of the GUM [4] to apply the MCM. In particular, the Mersenne-Twister pseudo-random number generator [10] was used in the numerical simulations of the input quantities dispersions of values.

Validated computational routines were used for the calculation of the average, mode, 95% expanded uncertainties (absolute, $U_{95\%}$, and relative, $U_{r\ 95\%}$) and computational accuracy, $U_{c\ 95\%}$, values, as well as the corresponding normalized histograms of the simulated output PDF's.

The results presented in Section 4 correspond to solutions that converge for 10^6 trials.

4. Results

4.1 Air density

Air density is an input quantity, not only for the local air velocity measurement, but also for the mass flow-rate. The numerical results obtained by MCM simulations are shown in Table 6, for which a Gaussian shape PDF was obtained.

Table 6: Air density simulation results.

Mean / kg·m^{-3}	Mode / kg·m^{-3}	$U_{95\%}$ / kg·m^{-3}	$U_{r\ 95\%}$ / %	$U_{c\ 95\%}$ / kg·m^{-3}
1,260 4	1,260 5	0,005 1	0,4	< 0,000 03

The performed sensitivity analysis revealed the main contributions for the obtained measurement uncertainty value: (i) the local static pressure (89%); (ii) the local temperature (8%); (iii) the molar constant of gas (3%); (iv) the molar mass and the gas deviation factor, with negligible contributions.

The adoption of extreme local pressure estimates of 80 000 Pa and 120 000 Pa do not produce significant changes in the obtained air density 95% expanded (absolute) measurement uncertainties, respectively, (0,960 0 ± 0,004 9) kg·m^{-3} and (1,440 6 ± 0,005 2) kg·m^{-3}. For a local temperature estimate variation, between 273 K and 373 K, the air density 95% expanded relative measurement uncertainty maintains a constant of 0,4%.

4.2 Compressibility correction factor

Based on the available input data and taking into account expression (4), the MCM simulations provided the results shown in Table 7, as well as the numerical PDF shown in Figure 1.

Table 7: Compressibility correction factor simulation results.

Mean	Mode	$U_{95\%}$	$U_{c\ 95\%}$
0,999 982 7	0,999 985 7	$3{,}6 \cdot 10^{-6}$	$< 7 \cdot 10^{-9}$

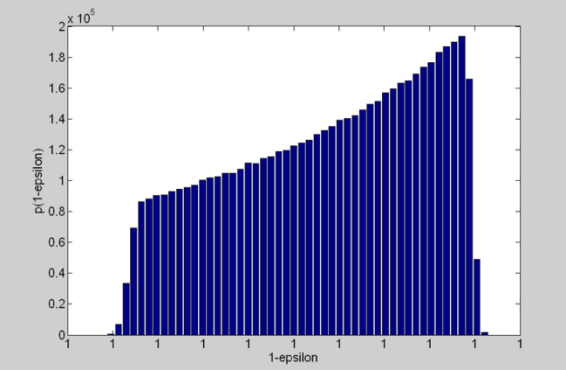

Figure 1: Numerical PDF of the compressibility correction factor.

The main contribution for the measurement uncertainty is related to the ratio of specific heat capacities (99,7%), which is also responsible for the obtained asymmetrical output PDF of the compressibility correction factor. This fact was confirmed by performing numerical simulations considering the specific heat capacities measurement uncertainty null, from which a Guassian shape PDF was obtained for the compressibility correction factor. The remaining input quantities (differential and local static pressures) have reduced contributions (0,15%) for the compressibility correction factor dispersion.

4.3 Local velocity

The measurement uncertainty propagation through expression (3) and the additional measurement uncertainty components shown in Table 3, allowed to obtain the local velocity results given in Table 8.

Table 8: Local velocity simulation results.

Mean / m·s^{-1}	Mode / m·s^{-1}	$U_{95\%}$ / m·s^{-1}	$U_{r\ 95\%}$ / %	$U_{c\ 95\%}$ / m·s^{-1}
3,983	3,978	0,069	1,7	< 0,000 4

The performed sensitivity analysis results given in Figure 2 allow to compare the weight of individual contributions to the combined measurement uncertainty.

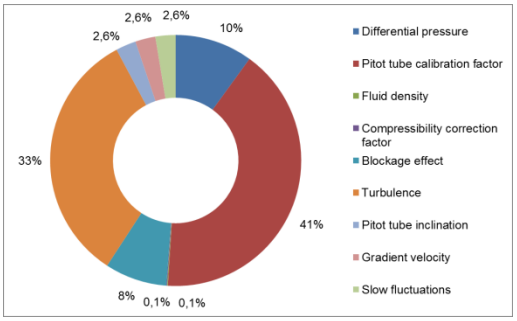

Figure 2: Relative weight of contributions to the local velocity combined measurement uncertainty.

Figure 2 shows two major contributions for the local velocity measurement uncertainty – the Pitot tube calibration factor (41%) and the turbulence and high frequency fluctuations uncertainty components (33%). A second group of intermediate contributions is related to the differential pressure measurement and the blockage effect uncertainty component, 10% and 8%, respectively, followed by a reduced contribution (2,6% each) concerning the Pitot tube inclination, gradient velocity, slow fluctuations uncertainty components. Both the fluid density and the compressibility correction factor have an almost null contribution (0,1% each) to the local velocity measurement uncertainty.

The numerical output PDF has a Gaussian shape, confirming the reduced influence of the compressibility correction factor (with a known asymmetric PDF – see Figure 1 – related to the specific heat capacities).

Additional simulations were performed, ranging local velocities from 4 m·s^{-1} up to 90 m·s^{-1}, showing a constant relative 95% expanded measurement uncertainty of 1,7%.

4.4 Volumetric flow-rate

Based on the results obtained in the previous Section 4.3, concerning the local velocity measurement, and taking into account the uncertainty components mentioned in Table 4 and the measurement uncertainty assigned to the cross-section area (see Table 2), the dispersion of volumetric flow-rate was obtained by numerical simulation, being characterized by a Gaussian PDF and by the results presented in Table 9, expressed both in $m^3 \cdot s^{-1}$ and $m^3 \cdot h^{-1}$

Table 9: Volumetric flow-rate simulation results.

Mean / $m^3 \cdot s^{-1}$	Mode / $m^3 \cdot s^{-1}$	$U_{95\%}$ / $m^3 \cdot s^{-1}$	$U_{r\ 95\%}$ / %	$U_{c\ 95\%}$ / $m^3 \cdot s^{-1}$
0,478 0	0,477 9	0,008 7	1,8	< 0,000 05
Mean / $m^3 \cdot h^{-1}$	Mode / $m^3 \cdot h^{-1}$	$U_{95\%}$ / $m^3 \cdot h^{-1}$	$U_{r\ 95\%}$ / %	$U_{c\ 95\%}$ / $m^3 \cdot h^{-1}$
1721	1720	31	1,8	< 0,18

The major contribution for the measurement uncertainty shown in Table 9 is related to the local velocity measurement uncertainty which contributes for 91% of the obtained dispersion of values. It is followed by the cross-section area measurement (4%) and the uncertainty components of integration technique (1,5%), the Pitot tube positioning (1,5%), the number of measurement points (1,5%) and the estimation of roughness coefficient (0,5%).

The numerical simulations were extended for a volumetric flow-rate measurement interval approximately between 0,15 $m^3 \cdot s^{-1}$ (544 $m^3 \cdot h^{-1}$) and 1,5 $m^3 \cdot s^{-1}$ (5440 $m^3 \cdot h^{-1}$), for which a constant relative 95% relative expanded measurement uncertainty of 1,8% was obtained.

4.5 Mass flow-rate

The results presented in Sections 4.1 (air density) and 4.5 (volumetric flow-rate) were used to perform the numerical simulations related to the mass flow-rate quantity. The obtained results, expressed both in $kg \cdot s^{-1}$ and $kg \cdot h^{-1}$, are shown in Table 10.

Table 10: Mass flow-rate velocity simulation results.

Mean / $kg \cdot s^{-1}$	Mode / $kg \cdot s^{-1}$	$U_{95\%}$ / $kg \cdot s^{-1}$	$U_{r\ 95\%}$ / %	$U_{c\ 95\%}$ / $kg \cdot s^{-1}$
0,602	0,603	0,011	1,8	< 0,000 06
Mean / $kg \cdot h^{-1}$	Mode / $kg \cdot h^{-1}$	$U_{95\%}$ / $kg \cdot h^{-1}$	$U_{r\ 95\%}$ / %	$U_{c\ 95\%}$ / $kg \cdot h^{-1}$
2167	2170	40	1,8	< 0,22

The measurement uncertainty provided is given, essentially, from the dispersion of the volumetric flow-rate (99%), while the contribution of the fluid density is negligible.

Additional numerical simulations were performed, ranging mass flow-rates from 0,2 $kg \cdot s^{-1}$ (720 $kg \cdot h^{-1}$) up to 2,0 $kg \cdot s^{-1}$ (7200 $kg \cdot h^{-1}$), showing a constant relative 95% expanded measurement uncertainty of 1,8%.

5. Conclusions

The MCM allowed to evaluate the flow-rate measurement uncertainty related to the use of Pitot tubes inside closed conduits, and to consider it fit-for-purpose.

Considering the studied measurement intervals, estimates and uncertainty components and adopted assumptions, the following 95% expanded relative measurement uncertainties were obtained: (i) 1,7%, for the local velocity quantity; (ii) and 1,8%, for both the volumetric and mass flow-rates. These values are close to the ones (1,4% and 1,5%, respectively) mentioned in [1].

The reduced difference (0,3%) between the results obtained from the conventional error approach, described in [1], and the MCM approach presented in this paper, is justified by the weak non-linearity of the applied mathematical models and by the low contribution of the measurement uncertainty of quantities, such as the compressibility correction factor, which are related to non-linear models. Therefore, the conventional approach can be used as a suitable approx. solution if the noticed differences are not significant for the target measurement accuracy.

This study showed that the local velocity quantity has a significant impact in the flow-rate measurement accuracy, in particular, the measurement uncertainty of the Pitot tube calibration factor and the uncertainty component related to turbulence and high frequency fluctuations. If needed, efforts to improve the flow-rate measurement accuracy should be directed towards these two elements, noticing that the corresponding quantification presented in this study is merely illustrative [1]. In a real case scenario, the probabilistic formulation and quantification must be confirmed and updated if required.

The results achieved are considered as able to provide useful information to be taken into account in a future revision of the ISO 3966 standard Annex G, namely, as an updated example of flow-rate measurement uncertainty calculation.

References

[1] ISO 3966: *Measurement of fluid flow in closed conduits. Velocity area method using Pitot static tubes*, 2008.
[2] JCGM 200: *International Vocabulary of Metrology (VIM) – Basic and general concepts and associated terms*, 2008.
[3] JCGM 100: *Evaluation of measurement data – Guide to the expression of Uncertainty in Measurement*, 2008.
[4] JCGM 101: *Evaluation of measurement data – Supplement 1 to the "Guide to the expression of Uncertainty in Measurement" – Propagation of distributions using a Monte Carlo method*, 2008.
[5] JCGM 102: *Evaluation of measurement data – Supplement 2 to the "Guide to the expression of Uncertainty in Measurement" – Extension to any number of output quantities*, 2011.
[6] Sydenham P H, *Handbook of Measurement Science. Volume 2. Practical Fundamentals* (John Wiley & Sons), 1983.
[7] Ower E, Pankhurst R C, *The Measurement of Air Flow* (Oxford, Pergamon), 1977.
[8] Sabersky R H, Acosta, A J, Hauptmann, E G, Gates, E M, *Fluid Flow* (New Jersey, Prentice Hall), 1999.
[9] NIST, CODATA Internationally recommended 2018 values of the Fundamental Physical Constants, https://physics.nist.gov/cuu/Constants
[10] Matsumoto M, Nishimura T, "Mersenne twister: a 623-dimensionally equidistributed uniform pseudo-random number generator", *ACM Transactions on Modelling and Computer Simulation*, **8**, 3-30, 1998.